Polarization Curves for an Alkaline Water Electrolysis at a Small Pin Vertical Electrode to Produce Hydrogen

Ph. Mandin
LIMatB EA4250, Université de Bretagne Sud, Centre de recherche rue de Saint-Maudé, BP 92116, 56321 Lorient Cedex, France

R. Wüthrich
Dept. of Mechanical and Industrial Engineering, Concordia University, Montreal, QC, Canada H3G 1M8

H. Roustan
Alcan - Centre de Recherche de Voreppe, 725 rue Aristide Bergès, BP 27, Voreppe Cedex 38341, France

DOI 10.1002/aic.12153
Published online January 20, 2010 in Wiley Online Library (wileyonlinelibrary.com).

During two-phase electrolysis for hydrogen production, according with alkaline–water electrolysis process, there are bubbles which are created at electrodes which imply a great hydrodynamic acceleration in the normal earth gravity field and then a quite important electrical properties and electrochemical processes disturbance, for both transport and reaction. This disturbance can lead to the modification of the local current density and to anode effects for example. In this work, a model experimental set-up is studied. The vertical pine electrode of small electro active surface area is surrounded with a large surface counter electrode. The hydrogen production is performed at the working electrode and effort is focused here upon the global electrochemical cell electrical performances. The polarization curves intensity vs. applied voltage are experimentally measured and presented for different factors such as: the electro active species concentration, nature and counter electrode diameter factors.
 AIChE J, 56: 2446–2454, 2010
Keywords: two-phase flow, water electrolysis, electrochemical modeling, bubbles

Introduction

Gas release and induced fluid flow at electrodes are characteristic for several electrochemical processes such as aluminum, fluorine, chlorine, and hydrogen production. The two-phase phenomena at gas evolving electrodes are in general neglected because of the major difficulty to be correctly taken into account. Nevertheless, nowadays, with the increasing interest in hydrogen production, clean, sustainable aluminum production and fluorine production for nuclear industry, these processes have to be revisited for further optimization.

The industrial two-phase electrolysis processes generally use vertical electrodes to promote bubble detachment and avoid gas accumulation. This is the reason why the present work focuses upon vertical electrodes. Previous works have shown the importance of the scale concerning the electrical properties behavior due to bubbles. In this work, the interest is focused upon small scale vertical pin electrode.

The classical alkaline water electrolysis has been chosen as a representative two-phase electrolysis process:

This work was presented at the 2009 conference of the French Chemical Engineering Society (Marseille, SFGP 2009).
Correspondence concerning this article should be addressed to Ph. Mandin at philippe.mandin@univ-ubs.fr.

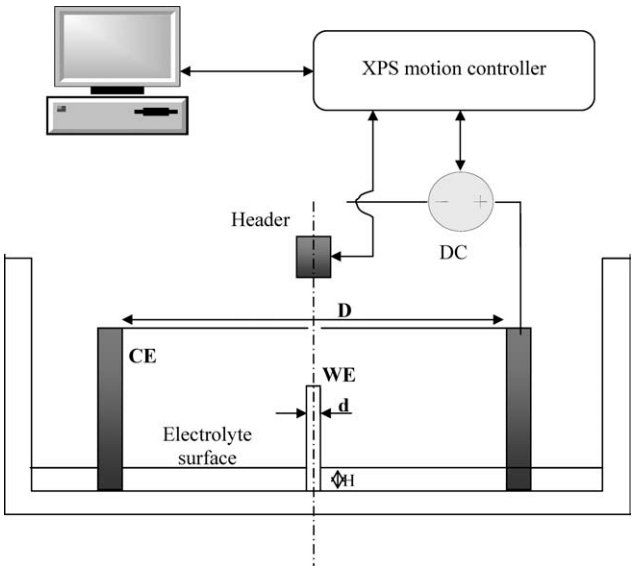

Figure 1. Experimental setup.

$$2\,H_2O + 2\,e^- \rightarrow H_2 + 2\,OH^-_{aq} \qquad E^\circ = -0.83\,V/ENH \tag{R1}$$

$$2\,OH^-_{aq} \rightarrow 0.5\,O_2 + H_2O + 2\,e^- \qquad E^\circ = 0.40V/ENH \tag{R2}$$

Note that the alkaline water electrolysis, with minimal cell voltage equal to 1.23 V, is generally chosen as the reference process for industrial hydrogen production. Typically, alternative processes such as the high temperature water vapor electrolysis or the Westinghouse processes are compared with it.[1]

Many researchers[1–15] have studied and exposed the difficulties in the two-phase electrolysis processes. The main problem is the existence of numerous effects, at the bubble scale but as well at the macroscopic electrochemical cell or reactor scale. They can be classified according surface and volume effects.

Surface effects are controlled by the electrode bubble surface coverage θ, the fraction covered by the adhering bubbles.[9–11] Consequences are multiple but all related to the fact that the actual available surface for mass and electron transfer is reduced. Vogt and his co-workers have studied several of these effects in stagnant and flowing electrolytes.[9–11] The flowing electrolyte considered was perfectly known, particularly in term of the wall shear stress. The stagnant electrolyte is rigorously obtained in absence of forced flow and gravity to avoid natural convection. This implies the interest in zero gravity experiments of many scientists.[7–14]

The volume effects are quantified by the gas void fraction ε affecting for example the effective species diffusion coefficient and the two-phase equivalent electrical conductivity according Bruggeman or Maxwell laws. A previous work has taken into account this volume effect in a computational fluid dynamic software calculation.[12]

Bubbles are as well motion sources for liquid electrolyte, due to Archimede force, and promote mass transport. This has a local impact and also a global one in the case of confined electrochemical reactors. The motion source near an electrode is transported in the reactor domain.[12–15]

In the present work, it is decided to study a small scale experimental vertical configuration with the aim to develop in the future what we call a "reduced model" (the flow motion is not calculated according Navier-Stokes equations). This kind of reduced model will offer a good validation case for more rigorous Navier-Stokes calculation.

This work focuses its interest upon the 1D interelectrode actual resistance of the two-phase electrolysis reactor. The small electrode height minimizes the natural induced flow. These experimental polarization characteristics measurements will allow the numerical validation for a given steady regime and also for the electrolysis cell properties sensitivity with explored factors. Experimental investigations are performed in order to establish the sensitivity with the electrolyte concentration, temperature and nature, working electrode nature, the geometrical factors, and the potential scan rate.

Experimental Setup and Qualitative Electrochemical Performances Behavior

Figure 1 shows the one dimensional experimental set-up with general geometrical parameters definition. The configuration is axis-symmetric for all input parameters chosen (see Table 1). The counter electrode has a large diameter $D = 70$ mm and a geometric surface area $S = \pi D{\cdot}H = 440$ mm^2 if $H = 2$ mm (height of both the electrolyte free surface and the immersed pin electrode). The stainless steel 316L working pin electrode is cylindrical with diameter $d = 0.4$ mm and a geometric surface area $s = \pi d{\cdot}H = 2.5$ mm^2 for an immerged length $H = 2$ mm.

In this configuration, the nominal current density at the counter electrode is two orders of magnitudes smaller than the nominal current density at the working electrode. The bubble evolution at the counter electrode may therefore be neglected as the over-potential will almost be zero.

In this work, following factors have been explored: the electrochemical cell applied potential, which is varying in time with scan velocity dV/dt, the electrolyte concentration, temperature and nature, the working electrode material, and the counter electrode diameter. Table 1 shows the different input factors explored and their chosen values. The goal is to establish steady polarization curve for each process conditions. This is done using multiple loops at a scan velocity value. This value is chosen sufficiently small to observe steady regime curves but also sufficiently large to ensure a small temperature increase due to Joule heating. The small

Table 1. List of the Experimental Parameters Explored

Parameters Study	Numbers of Level	Values Explored
Radius of counter-electrode (D/2)	3	35, 25, and 15
Material of working-electrode	3	Stainless steel, carbon steel, graphite
Type of electrolyte	2	NaOH and KOH
Voltage speed, dV/dt	3	30, 20, and 10 V/s
Initial temperature of the electrolyte, T	5	23, 32, 54, 62, and 80°C

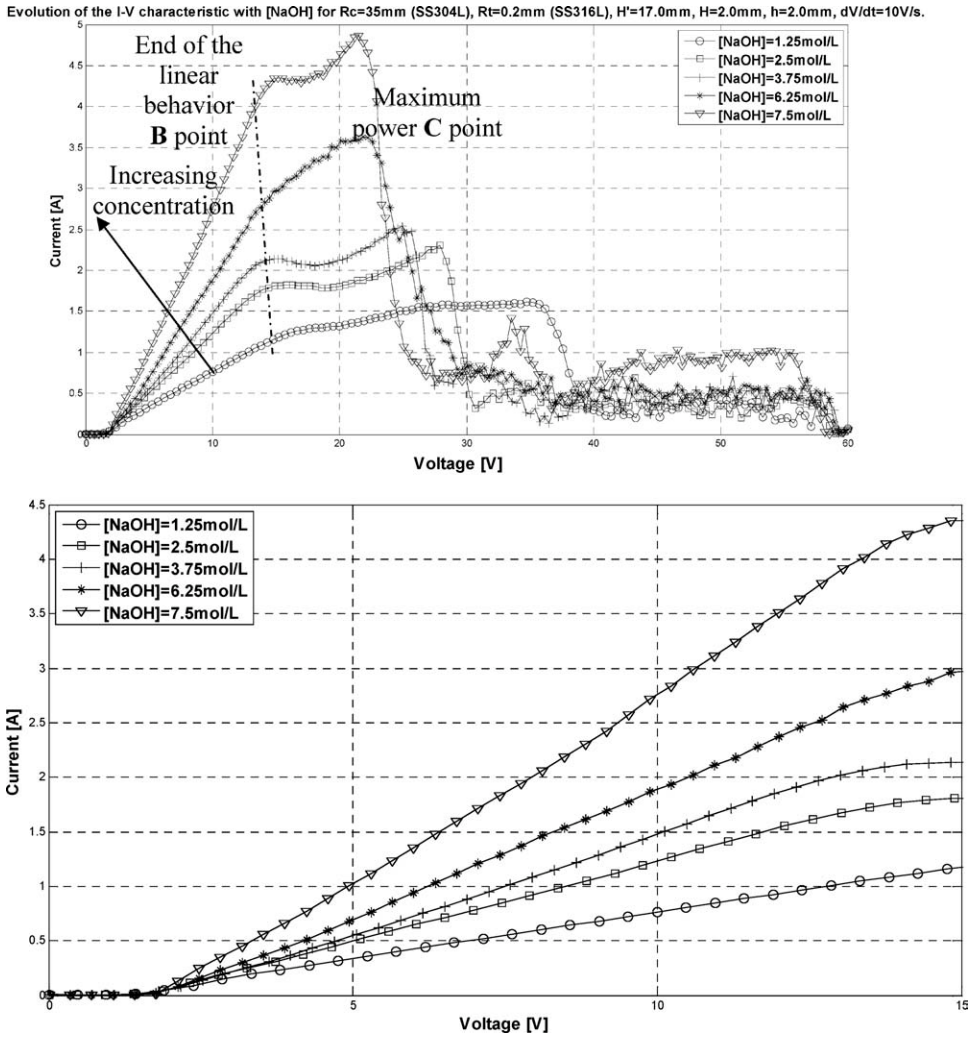

Figure 2. Evolution of the I-V characteristic with NaOH electrolyte for various concentration.

$D = 70$ mm, $d = 0.4$ mm, stainless steel working electrode (SS304L), $H = 2$ mm, and $dV/dt = 10$ V/s. General polarization curve (top) and focus on the linear part (botom).

influence of this last effect has been controlled using large number of loops: though a larger temperature at the loop end than at the loop beginning, the polarization curves remain identical.[13]

Figure 1 shows the one dimensional configuration experimental set-up.

Because of the important potential and current values, a two electrode experimental setup is chosen. A computer-controlled stabilized potential source has been used. The displacement of the working electrode is ensured by a computer-controlled Newport micrometer stage. The immersion of the electrode was estimated with 0.1 mm precision. The electrolyte aqueous solution is prepared with NaOH ranging from 5 to 30 wt % mass fraction. Data were computer recorded.

This 1D geometrical configuration has been chosen to allow the use of a simple 1D electrical resistance model and to be under the rigorous 1D assumption to be sure of the investigated factors influence upon equivalent ohmic resistance.

Figure 2 shows for various NaOH concentrations mean polarization curves (potential-current characteristics obtained with 50 successive scans) for $H = 2$ mm, $dV/dt = 10$ V/s, $T = 23°C$.

After reaching the water decomposition potential in the chosen condition (between 2 and 2.5 V), the cell current follows a quasi linear increase until the cell terminal voltage U_B (about 15 V) associated with current I_C, at the linear end behavior point called B (Figure 2, top). Nevertheless, after this linear behavior, there is a small but reproducible nonlinear resistance increase, mainly due to the increase of the number of bubbles in the electrode vicinity and even though the temperature is increasing due to Joule heating during the experiment. This last temperature increase effect has demonstrated previously[13] and with the loop measurements and treatment, is locally strong but small at the cell scale.

Figure 3 shows the bubbles accumulation around the working electrode during electrolysis for two applied voltage values (7.5 and 12.5 V). The bubble disposition has an inverted pyramid shape due to the Archimede force. These

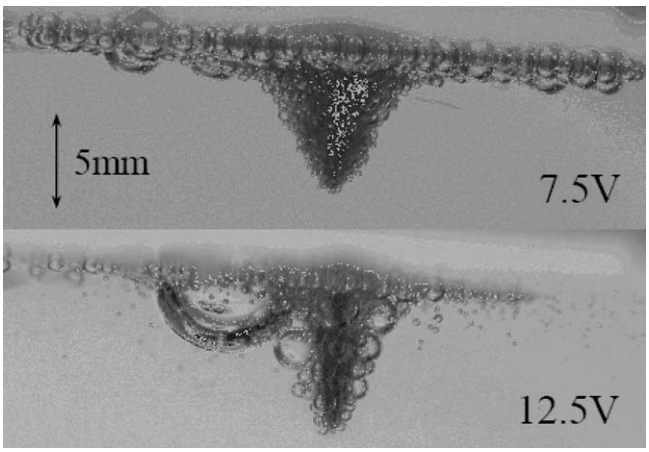

Figure 3. Evolution of the bubbles "inverted pyramide shape" disposition around the working electrode for two different values of the applied voltage.

$D = 70$ mm, $d = 0.4$ mm, steel working electrode (SS304L), $H = 2$ mm, and $dV/dt = 10$ V/s.

photographs show a regular bubble accumulation, with no coalescence phenomena, and then the bubbles contacts can be supposed regular, at least at these voltages. This two-phase layer will be considered as a rigid spheres stacking and leads to known porosity values. For larger cell terminal voltage, this regularity is lost as it can be seen on Figure 3 (bottom).

For increasing cell voltages, the linear behavior of the current is lost. The current still increases slightly up to a maximal value called I_C associated to a cell voltage called U_C at point C (Figure 2 top). The resistance is increasing due to the increased number of bubbles. For large cell voltage values, the current standard deviation becomes more and more important. This is certainly due to bubbles evolving dynamics: there is a spatial nucleation sites distribution and also an unsteady bubbles departure frequency which lead to large standard deviation around the mean current value. This is the reason why we have focused our attention for processes with smaller than 15 V applied voltage to observe linear current increase with small standard deviation values.

The exact mechanism leading to this plateau is not yet elucidated. It is not due to electro active species diffusion limitation because at the working electrode water species reactions are involved. A possible mechanism is the limitation of the bubble release from the electrode surface due to their increasing size obtained by coalescence.[13]

After point C, the mean current decreases sharply. This is associated to the surface and volume screening roles of bubbles which have led to a continuous gaseous film around the working electrode.[13–20] The electro-active area fraction screened by the adhering bubbles is defined as θ, whereas the bubble volume fraction in the surrounding electrolyte is noted ε. The bubbles evolving leads first to a mass transfer increase effect which, for larger imposed cell potential value, is followed by a transition regime. First the current passes through the free of bubble surface area $(1-\theta)$.S. Second, a smaller but non zero intensity passes through the continuous gaseous film. This first occurs with glow discharges and second with spark discharges.[1,2,13] With increasing cell potential, the bubble coverage fraction θ increases as well and eventually reaches almost one or smaller critical value (continuous hydrogen gaseous film). However, movies and photographs exploitations show that the electrochemical reaction continues to occur though the appearance of total coverage.[2–13]

After this complete qualitative description of the process behavior for large imposed potential values, this work is going to focus upon the current transfer before the formation of a gas film, in the smaller than 14 V region, with the linear current increase. The practical goal of this experimental quantitative investigation is to identify validation data base for in progress two-phase electrolysis modeling work.

Quantitative Experimental Results

Interelectrode resistance sensitivity with concentration

This small 1D configuration has been chosen in order to be allowed to use a simple 1D electrical resistance model and then to be sure of the investigated factors influence upon what is called here "the equivalent electrical conductivity."

In absence of bubbles, the primary current density distribution has no vertical gradients and is obeying to the 1D-axis symmetry expression:

$$U_{\text{applied}} = R_{\text{theo}} I_{\text{resulting}} \qquad \text{with :} \quad R_{\text{theo}} = \ln(D/d)/(2\pi h\sigma) \tag{1}$$

R_{theo} is the inter-electrode resistance (Ω) for pure ohmic electrolyte (absence of convecto-diffusive transport and bubbles).[17–19] Electrical conductivity σ (S/m) of NaOH is given in Table 2.

The experimentally measured resistance R_{exp} has been estimated from the experimental polarization curves (mean I-U characteristics) and an experimental electrical conductivity σ' (S/m) has been computed using Eq. 1. Table 2 shows this estimation for various NaOH concentrations. As expected, the discrepancy between theory and experiment is very large, particularly for high concentrations. The electrolyte can't be modeled as purely "ohmic." Furthermore, the evaluated electrical conductivity is constantly increasing with electrolyte concentration, which is contrary to the published data. One has to conclude that the simple model (1) is not able to describe the inter-electrode resistance, even not qualitatively.

Table 2. Resistance Evolution of NaOH Electrolyte for $dV/dt = 10$ V/s, $H = h = 2.0$ mm 1D Case, Stainless Steel at $T = 23°C$

Wt (%)	5	10	15	25	30
Concentration (mol/L)	1.25	2.5	3.75	6.25	7.5
Conductivity, σ (S/m) (after [19])	27	35	41	37	31
R_{exp} (Ω)	11.7	7.1	6	4.4	3
R_{theo} (Ω)	15.2	11.7	10	11.1	13.3
Conductivity σ'(S/m)	35	58	69	93	137
Discrepancy (%)	30	65	67	152	342
$R_{\text{theo}'}$ (Ω)	20	15	13	14	17
$R_{\text{cv-dif}}$ (Ω)	51	18	15	7	4

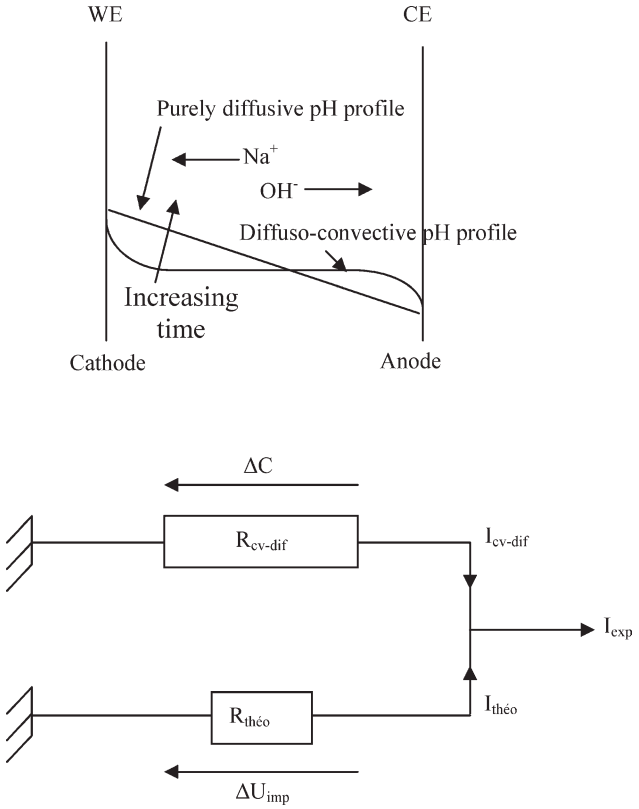

Figure 4. Ions profile between working electrode and counter electrode (top) and equivalent electrical circuit modeling (bottom).

In fact, there is a two-phase bubble layer, with thickness δ and void fraction ε, at the working electrode surface, and a resistance term, should be added to the R_{theo} expression according with (2):

$$R'_{\text{theo}} = \ln(1 + 2\delta/d)/(2\,\pi.h\sigma'') + \ln(D/(d + 2\delta))/(2\pi h.\sigma) \tag{2}$$

with the two-phase equivalent electrical conductivity given by Bruggeman's law:

$$\sigma'' = \sigma.(1 - \varepsilon)^{1.5} \tag{3}$$

This expression is a better modeling of the actual situation. Dissolved hydrogen gas immediately yields, after the electrolysis beginning, to bubbles nucleation and growth. Input parameters δ and ε are difficult to estimate.

Nevertheless, Eq. 2 should lead to larger electrical resistances than Eq. 1 as shown in Table 2 (illustrated with $\delta = 10^{-4}$ m, and $\varepsilon = 0.64$; centered cubic disposition is assumed). Table 2 also shows that the equivalent resistance is larger than the experimental value for each electrolyte concentration. If the bubble partial surface screening effect was considered, the resistance would even increase further.

The model discrepancy is increasing with the electrolyte bulk concentration C°. It is well known that the higher the ion concentration is, the more the electro migration is negligible. This demonstrates that the ohmic model alone, generally used for electrochemical engineering calculations and cells designs, which takes only into account the electro migration species transport (primary modeling), is not accurate. The computed resistances are over estimated compared with the measured one. The species transport due to diffusion and convection must be considered.

Figure 4 (top) shows the behavior in time of the pH profile and the one of OH^- and Na^+ concentration. The non-electro migration transport may be mainly diffusive and the linear profile will be obtained in case of sufficient large times, once the steady regime reached and in absence of convective transport.

Then, according with Eq. 1, it can be defined to current transport:

$$I_{\text{resulting}} = U_{\text{applied}}/R_{\text{exp}} = I_{\text{electromigration}} + I_{\text{cv-dif}} \tag{4}$$

and $R_{\text{cv-dif}}$ is actually defined as:

$$R^{-1}_{\text{cv-dif}} = R^{-1}_{\text{exp}} - R^{-1}_{\text{ohm}} \tag{5}$$

and is given in Table 2 (last line). The equivalent electrical circuit is shown in Figure 4 (bottom). For the largest concentration value of NaOH (7.5 M), $R_{\text{ohm}} = 13.3\ \Omega$ instead of $R_{\text{exp}} = 3\ \Omega$ which leads to $R_{\text{cv-dif}} = 4\ \Omega$. As it can be seen, charge transport phenomenon importance is increasing with concentration.

Figure 5 shows that the convecto-diffusive resistance $R_{\text{cv-dif}}$ (Ω) sensitivity with electrolyte concentration C (M) for larger concentration values than 1.25 M is linear. This is true as soon as the electro migration can be neglected. It experimentally appears that:

$$\partial R_{\text{cv-dif}}/\partial C = -2.9\,\Omega/\text{M} \tag{6}$$

The sensitivity of the cell resistance with the concentration is then quantitatively estimated. The bulk electro active species OH^- is reacting at the anode, the counter electrode (CE) with large surface. The current density at the CE is supposed to be small and then no diffusion limitation should

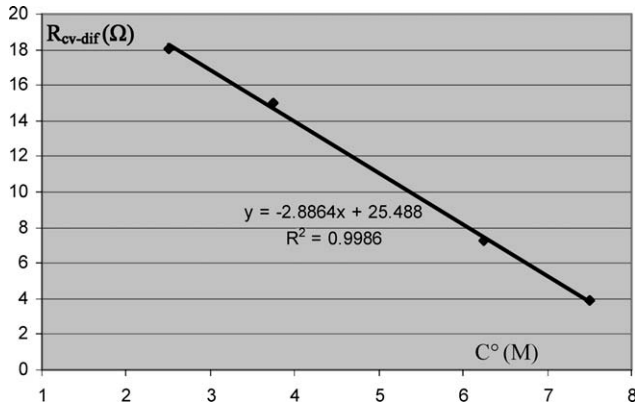

Figure 5. Linear evolution of the convecto-diffusive transport resistance $R_{\text{cv-dif}}$ (Ω) with the NaOH concentration C° (M).

$D = 70$ mm, $d = 0.4$ mm, steel working electrode (SS304L), $H = 2$ mm, and $dV/dt = 10$ V/s.

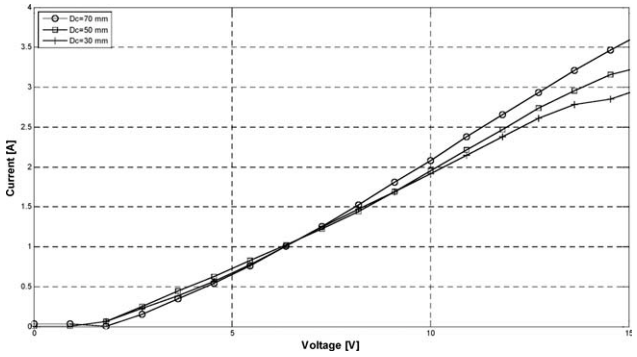

Figure 6. Evolution of the I-V characteristic with KOH electrolyte for various counter electrode diameter D.

$d = 0.4$ mm, steel working electrode (SS304L), $H = 2$ mm, and $dV/dt = 20$ V/s^{-1}.

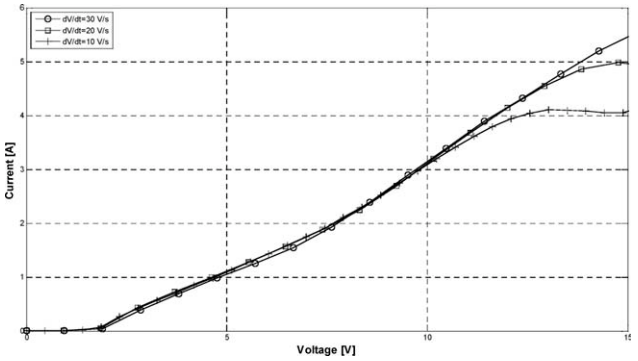

Figure 7. Evolution of the I-V characteristic with KOH electrolyte for various scan velocity *dV/dt*.

$D = 70$ mm, $d = 0.4$ mm, steel working electrode (SS304L), $H = 2$ mm, and $C = 7.5$ M.

occur, particularly for properties measured near the electrolysis potential. It is difficult to give explanations without numerical investigation, which is now in progress. However, the linear property will be an important experimental evidence for numerical modeling validation.

Interelectrode resistance sensitivity with counter electrode diameter

Experiments have been performed with different counter electrode diameters $D = 70$, 50, and 30 mm. According to Eq. 2, the ohmic resistance R_{ohm} is increasing with diameter D. However, Figure 6 shows that the experimental resistance R_{exp} is almost independent of the diameter D for small cell terminal voltages and is increasing with it for larger terminal voltages. According to Figure 6, R_{exp} is constant for varying counter electrode diameters: the experimental resistance is mainly determined by the near working electrode (WE) phenomena, the electrochemical kinetics because reaction feeding in water, should involve no diffusion limitation. According to Table 2, $R_{\text{cv-dif}}$ is decreasing with increasing diameter D:

$$\partial R_{\text{cv-dif}}/\partial D = -0.15\,\Omega/\text{mm} \tag{7}$$

Interelectrode resistance sensitivity with scan rate

The cell potential scan rate dV/dt (V/s) has also been explored to evaluate the quantitative results reproducibility. The chosen values are small enough to ensure steady polarization curves measurements but large enough to ensure, with 50 loops, a small temperature increase. The results are shown in Figure 7. There is a large difference of the order of magnitude of the different involved phenomena time constants, but for the range explored, there is no sensitivity. The theoretical ohmic resistance, established under steady regime assumption, is itself nonscan velocity dependent. Then, Figure 7 clearly shows that the convecto-diffusive resistance slope is not a function of the cell potential scan rate and:

$$\partial R_{\text{cv-dif}}/\partial(dV/dt) = 0 \tag{8}$$

Table 3. Evolution of Experimental Resistance for NaOH and KOH Electrolytes for Various Concentration

% wt KOH	7	14	21	35	42
% wt NaOH	5	10	15	25	30
C° (M)	1.25	2.5	3.75	6.25	7.5
R_{exp} NaOH (Ω)	11.7	7.1	6.0	4.4	3.0
R_{exp} KOH (Ω)	10	8.3	5.8	4	2.7

$D = 70$ mm, $d = 0.4$ mm, steel working electrode (SS304L), $h = H = 2$ mm, and $dV/dt = 10$ V/s.

Interelectrode resistance sensitivity with electrolyte species

Figure 8 shows the evolution of the polarization curves when KOH is used as electrolyte in place of NaOH. The electrolyte concentration chosen are the same as these chosen for NaOH. The mass weight fraction is different as shown in Table 3 but the concentration is identical for each of the five experiments. According with handbooks data, the KOH electrical conductivity is similar to the one of NaOH. At 25°C for C° $= 10^{-2}$ M, $\sigma_{\text{NaOH}} = 0.2379$ S/m whereas $\sigma_{\text{KOH}} = 0.228$ S/m. For concentration smaller than 10 wt %, the electrical conductivity of both electrolyte solutions is identical. For mass fraction larger than 10 wt %, KOH has a larger electrical conductivity than NaOH. The maximal KOH

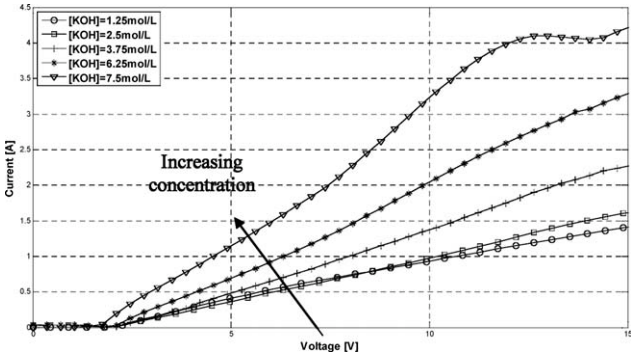

Figure 8. Evolution of the I-V characteristic with KOH electrolyte for various concentration.

$D = 70$ mm, $d = 0.4$ mm, steel working electrode (SS304L), $H = 2$ mm, and $dV/dt = 10$ V/s.

Table 4. Evolution of the Electrical Resistance with the Initial Electrolyte Temperature

Initial Temperature (°C)	Experimental Resistance (Ω)
22	12.4
32	10.7
58	6.9
64	6.4
80	5.1

NaOH, $C^\circ = 1.25$ M, 20 V/s.

electrical conductivity is about 55 S/m at 25 wt % compared to 41 S/m at 15 wt % for NaOH. This is mainly due to the ions Na^+ and K^+ mass difference which have not the same ion radius: 1.133 nm for K^+ instead of 1.095 nm for Na^+. Table 3 shows that R_{exp} for KOH is always smaller (only wrong in the case of 14 wt %) than the NaOH associated resistance. This is in good accord with the handbook electrical conductivities for both KOH and NaOH.

Figure 9 compares the characteristics obtained in NaOH and KOH solutions. As seen in Table 3, the slope is almost identical but not the end of linearity region (called point B) and the value of the limiting current, which is lager for KOH. This can be due to the larger Arrhenius viscosity and larger Pelofsky surface tensions values for KOH electrolyte. The bubbles, for a given gas volume, are larger for KOH and the friction force is more important. Consequently, electrode surface screening is smaller. It is to notice that for large values of the imposed voltage (larger than U_C), it appears spark discharges which are yellow for the NaOH electrolyte and purple for KOH, according with their atomic spectroscopy properties.

Interelectrode resistance sensitivity with initial electrolyte temperature

Figure 10 and Table 4 shows the inter electrode resistance in function of the different initial electrolyte temperatures. The Figure 10 shows the slope evolution with initial temperature for NaOH 1.25 M (5 wt %). The resistance decreases with the temperature level. It has been verified that, even for the 50 loops performed, the temperature increase during

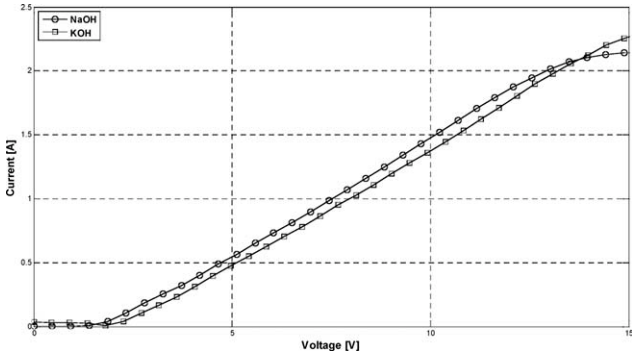

Figure 9. Comparison of the I-V characteristic with NaOH and KOH electrolyte.

$C^\circ = 3.75$ M, $D = 70$ mm, $d = 0.4$ mm, steel working electrode (SS304L), $H = 2$ mm, and $dV/dt = 10$ V/s.

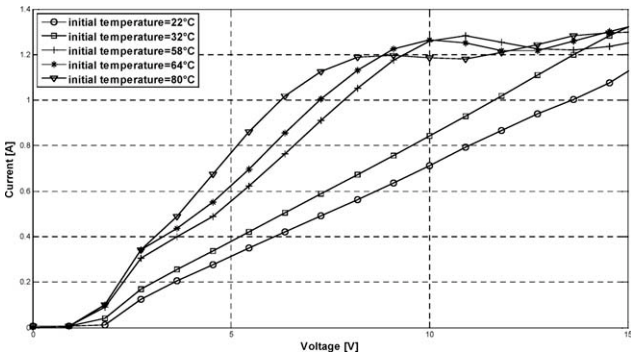

Figure 10. Evolution of the I-V characteristic with the electrolyte temperature.

NaOH with $C^\circ = 1.25$ M, $D = 70$ mm, $d = 0.4$ mm, $H = 2$ mm, and $dV/dt = 20$ V/s.

experiment is small enough to consider that the experiments occur with constant temperature equal to the initial one.

Table 4 shows that the experimental resistance is decreasing with temperature which is in good accord with the species diffusion coefficient increase with temperature. It was also observed a decrease of U_B and of the limiting current. Because the viscosity is decreasing with temperature, hydrodynamic friction is smaller and growing bubbles are larger.

Interelectrode resistance sensitivity with working electrode material

Figure 11 shows the effect of the working electrode material upon the experimental resistance R_{exp}. The measured resistance is smaller for stainless steel and larger for graphite. Table 5 gives quantitatively this evolution with the working electrode material. The porosity and roughness is larger for graphite than for stainless steel. The resistance evolution is directly related to the bubbles accumulation at the electrodes. Graphite offers much more nucleation sites for bubbles than stainless steel, which has a smoother surface. The quantitative electrode material analysis and diagnostic are in progress.

Discussion

Scan velocity and loops number

The high scan velocity (sweep rate) has been chosen to minimize the temperature evolution at electrode due to Joule heating. Previously, published works[13,20] have shown that the capacitive impedance can be neglected during these processes. The demonstration was obtained with much smaller scan velocity, which was leading to same results.

Table 5. Evolution of U-I Properties for the Three Explored Working Electrode Materials NaOH, $C^\circ = 3.75$ M, $h = H = 2$ mm, 20 V/s

Material	R_{exp} (Ω)	I_B (A)	U_B (V)	I_C (A)	U_C (V)
Stainless steel SS304L	5.2	2.27	14.58	2.73	25.61
Carbon steel	6.2	1.94	14.62	2.19	24.89
Graphite	8.3	1.41	13.92	1.65	22.55

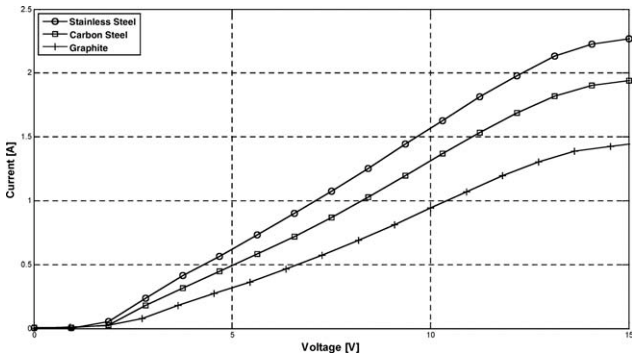

Figure 11. Evolution of the I-V characteristic with the working electrode material.

NaOH with $C^\circ = 3.75$ M, $D = 70$ mm, $d = 0.4$ mm, $H = 2$ mm, and $dV/dt = 20$ V/s.

To illustrate the importance of the scan velocity, the loops number, the temperature increase and the experiment duration, and many other experiments have been performed for a similar experimental setup to identify the experimental parameter to use. Many loops have been performed and the resistances have been calculated at the beginning and at the end of the experiments to estimate the slope change during the experiments.

Five representative experimental results are given in the Table 6.

The experiment duration is the larger voltage interval value times the loop number. For example for the test0 the duration is $35 \times 10 = 350$ s.

It appears with this additional work:

1. The larger change between resistance at the beginning and at the end is obtained for the larger excursion in the wider voltage intervals (0–35) V. This is the reason why experiments of the linear zone have been limited to (0–15) V.

2. At the end of loops the $R_{exp,end}$ is generally smaller than the initial one $R_{exp,init}$; this is due to the Joule heating during sufficiently longtime experiments. The only exception is obtained for the smaller experiment duration (test 1).

From this experimental parameters investigation, it has been possible to choose adapted experiments condition to obtain reproducible resistance values, even after loops.

Temperature influence

The temperature influence is difficult to model but seems to be limited. The temperature increase is mathematically modeled with the local energy balance:

$$\rho.c_P.\partial T/\partial t + \rho.c_P.y_z \,\mathrm{grad}\, T = \partial(\lambda \partial T/\partial x)/\partial x + j^2/\sigma \quad (9)$$

ρ is the density in (kg/m^3), c_P is the heat capacity (J/kg K), T is the temperature (K), t is time (s), x and z are horizontal and vertical coordinates (m), respectively, v_z (m/s) is the vertical velocity, λ (W/m K) is the heat conduction coefficient and the local Joule heating is j^2/σ.

a. The heat is mostly generated at the WE interface and is not exchanged with electrolyte neighbor; under this assumption, the temperature increase is very large:

$$s = 5.5\,\mathrm{mm}^2 = 5.5\ 10^{-6}\mathrm{m}^2 \text{ and } \mathrm{R.I} = t.dV/dt$$

$$j = I/s = t.dV/dt/(R.s) = 10^6 \mathrm{A/m}^2$$

$$dT/dt = 10^{10}/10^6 = 10^4 \mathrm{K/s}$$

This hypothesis leads to unrealistic temperature value.

b. The heat is mostly generated at the WE interface and is exchanged everywhere in the confined electrochemical cell only with diffusive heat transfer (no convection); under this assumption, the temperature increase is smaller but large.

c. The heat is mostly generated at the WE interface and is exchanged everywhere in the confined electrochemical cell only with both diffusive and convective heat transfer (due to natural convection and bubbles evolving). To calculate the temperature increase under this assumption, a dedicated two-phase induced flow due to bubbles evolving numerical modeling is needed; this work is on progress.

d. The heat is mostly generated at the WE interface but is supposed to be exchanged everywhere immediately in the confined electrochemical cell; under this assumption, the temperature increase is smaller than 1 K. The actual modeling is of course "*c*" which becomes "*d*" for large intensity and bubble evolving, due to the intense stirring.

The electrical conductivity is increasing with temperature, and then, the resistance decreases with time and with voltage. In Table 7, the experimental resistance is generally smaller at the experiment end than at the beginning. However, the change is really small, even after numerous loops (between 10 and 50).

The electrical conductivity evolution with temperature is known,[19,20] for such alkaline electrolytes, to be really small: $d\sigma/dT < 0.05/5 = 10^{-2}$ S/m K

And then the cell resistance sensitivity with temperature can be estimated:

$$dR/dT = R/\sigma.d\sigma/dT < 15.2/27\ .\ 10^{-2} = 5.6\ 10^{-3}\mathrm{Ohm/K}$$

Experimentally, it can be estimated from the Figure 10 that from 22 to 32°C, the resistance decrease is (8.33–7.14) Ohms, and leads to $dR/dT = -0.12$ Ohm/K.

Then, the temperature increase at the end of the numerous loops performed, for one given initial temperature level, has

Table 6. Complementary Tests Performed to Estimate the Experimental Resistance Sensitivity with the Factors Scan Rate, Number of Loops, Experiment Duration, and Relative Heating Effects

	$R_{exp,init}$	$R_{exp,end}$	Change (%)	Duration (s)
test0: 0–35 V; 1 V/s; 10 loops	11.4	8.26	−27.5%	350
test1: 0–5 V; 1 V/s; 50 loops	11.7	12.6	7.7%	250
test2: 0–10 V; 1 V/s; 50 loops	12.2	10.7	−12.3%	500
test3: 0–5 V; 0.1 V/s; 20 loops	13.5	12.8	−5.2%	1000
test4: 0–35 V; 1 V/s; 50 loops	13.9	10.7	−23.0%	1750

a small impact upon the calculated resistance. The initial temperature value is a more important factor than the temperature increase during loops.

Material influence

Three different materials (stainless steel, carbon steel, and carbon) have been investigated in the present work and leads to different resistance value. This is not due to the unstability of the WE material but due to the difference in the nucleation-growth of hydrogen bubbles for materials with different chemical composition and micro to nanostructure. For example, the hydrophobic electrodes are known with Vogt work[9,10] leads to a small wettability of the produced bubbles and then to a smaller screening and resistance for current transport. In our opinion, this is mostly this effect which leads to different slopes for the three explored materials.

Conclusions

This work has demonstrated that for a small dimension 1D vertical axis symmetrical pine electrode, the purely ohmic resistance models, for the factors explored (electrolyte nature, composition or temperature, working electrode material, counter electrode diameter) are over estimating the experimentally measured electrical resistance. Even if a Bruggeman ohmic resistance is introduced to model the charge transport in the two-phase boundary layer no improvement can be achieved. For these small scale conditions, it appears that primary or secondary current distribution models are as well inaccurate to describe the actual electrochemical performances. The mass transport, due to diffusion and convection, appears to be, at this scale, a more important phenomenon for an accurate model than the volume or surface screening due to bubbles. This greater importance of the bubbles mass transport enhancement had already been demonstrated with the use of electrochemical impedance spectroscopy by Gabrielli et al. who have defined what is now called the local ''quenching mass flux'' and of course the macroscopic convective transport due to bubbles motion. It appears at the end of this work as really important to develop a two-phase flow numerical modeling to describe both heat and mass transport from the working electrode vicinity to the bulk and to access to the actual interface condition for the electrochemical reaction.

Acknowledgments

Authors would like to thank the French Research National Agency (ANR) and the Natural Sciences and Engineering Research Council of Canada (NSERC) for their financial support. The French Spatial Studies National Center (CNES) is also acknowledged.

Literature Cited

1. Jomard F, Feraud JP, Caire JP. Numerical modeling for preliminary design of the hydrogen production electrolyzer in the Westinghouse hybrid cycle. *Int J Hydrogen Energy*. 2008;33:1142–1152.
2. Kellogg H. Anode effect in aqueous electrolysis. *J Electrochem Soc*. 1950;97:133–142.
3. Azumi K, Mizuno T, Akimoto T, Ohmori T. Light emission from Pt during high-voltage cathodic polarization. *J Electrochem Soc*. 1999; 146:3374–3377.
4. Janssen LJJ, Hoogland JG. The effect of electrolytically evolved gas bubbles on the thickness of the diffusion layer. *Electrochim Acta*. 1970;15:1013–1023.
5. Janssen LJJ, Sillen CWMP, Barendrecht E, Van Stralen SJD. Bubble behaviour during oxygen and hydrogen evolution at transparent electrodes in KOH solution. *Electrochim Acta*. 1984;29:633–642.
6. Korobeinikov SM, Melekhov AV, Sinikh Yu N, Soloveichik Yu G. Effect of strong electric field on the behaviour of bubbles in water. *High Temp*. 2001;39:368–372.
7. Matsushima H, Nishida T, Konishi Y, Fukunaka Y, Ito Y, Kuribayashi K. Water electrolysis under microgravity. I. Experimental technique. *Electrochim Acta*. 2003;48:4119–4125.
8. Matsushima H, Fukunaka Y, Kuribayashi K. Water electrolysis under microgravity. II. Description of gas bubble evolution phenomena. *Electrochim Acta*. 2006;51:4190–4198.
9. Vogt H, Aras Ö, Balzer RJ. The limits of the analogy between boiling and gas evolution at electrodes. *Int J Heat Mass Transfer*. 2004;47:787–795.
10. Vogt H, Balzer RJ. The bubble coverage of gas-evolving electrodes in stagnant electrolytes. *Electrochim Acta*. 2005;50:2073–2079.
11. Eigeldinger J, Vogt H. The bubble coverage of gas-evolving electrodes in a flowing electrolyte. *Electrochim Acta*. 2000;45:4449–4456.
12. Mandin Ph, Hamburger J, Bessou S, Picard G. Calculation of the current density distribution at vertical gas-evolving electrodes. *Electrochim Acta*. 2005;51:1140–1156.
13. Wüthrich R, Hof LA, Lal A, Fujisaki K, Bleuler H, Mandin Ph, Picard G. Physical principles and miniaturization of spark assisted chemical engraving (SACE). *J Micromech Microeng*. 2005;15:268–275.
14. Mandin Ph, Roustan H, Wüthrich R, Hamburger J, Picard G. Two-phase electrolysis process modelling: from the bubble to the electrochemical cell scale. In: *Simulation of Electrochemical Processes II. Transactions on Engineering Sciences*. Carlos Brebba, editor, Southampton, U.K.: WIT Press, 2007:73.
15. Mandin Ph, Ait Aissa A, Roustan H, Hamburger J, Picard G. Two-phase electrolysis process: from the bubble to the electrochemical cell properties. *Chem Eng Process: Process Intensification*. 2008;47: 1926–1932.
16. Gabrielli C, Huet F, Nogueira RP. Fluctuations of concentration overpotential generated at gas-evolving electrodes. *Electrochim Acta*. 2005;50:3726–3736.
17. Bard AJ, Faulkner LR. *Electrochemical Methods-Fundamentals and Applications*, 2nd ed. New York: Wiley, 2001:243.
18. Lapicque F. Electrochemical engineering: an overview of its contributions and promising features. *Chem Eng Res Des*. 2004;82:1571–1574.
19. Zaytsev I, Aseyev G. *Properties of Aqueous Solution of Electrolytes*. Boca Raton: CRC Press, 1992.
20. Wüthrich R, Comninellis Ch, Bleuler H. Bubble evolution on a vertical electrode under extreme current densities. *Electrochim Acta*. 2005;50:5242–5246.

Manuscript received Jun. 12, 2009, and revision received Nov. 18, 2009.